



A 3D MHD-Particle Tracing Model of Na⁺ Energization on Mercury's Dayside

Austin N. Glass, Jim M. Raines, Xianzhe Jia, Valeriy Tennishev, Yinsi Shou,
Sae Aizawa, James A. Slavin

► To cite this version:

Austin N. Glass, Jim M. Raines, Xianzhe Jia, Valeriy Tennishev, Yinsi Shou, et al.. A 3D MHD-Particle Tracing Model of Na⁺ Energization on Mercury's Dayside. *Journal of Geophysical Research Space Physics*, 2021, 126, 10.1029/2021JA029587 . insu-03672357

HAL Id: insu-03672357

<https://insu.hal.science/insu-03672357>

Submitted on 6 Aug 2022

HAL is a multi-disciplinary open access archive for the deposit and dissemination of scientific research documents, whether they are published or not. The documents may come from teaching and research institutions in France or abroad, or from public or private research centers.

L'archive ouverte pluridisciplinaire **HAL**, est destinée au dépôt et à la diffusion de documents scientifiques de niveau recherche, publiés ou non, émanant des établissements d'enseignement et de recherche français ou étrangers, des laboratoires publics ou privés.

Copyright

JGR Space Physics

RESEARCH ARTICLE

10.1029/2021JA029587

Key Points:

- Sodium ions (Na^+) with initial energy of 1 eV are energized by Dungey cycle return flow in the dayside dipolar region
- Na^+ are not trapped within the dayside dipolar region of Mercury
- One- and two-stage pickup processes can energize Na^+ up to tens of keV entirely on the dayside

Supporting Information:

Supporting Information may be found in the online version of this article.

Correspondence to:

A. Glass,
anglass@umich.edu







Citation:

Glass, A. N., Raines, J. M., Jia, X., Tennishev, V., Shou, Y., Aizawa, S., & Slavin, J. A. (2021). A 3D MHD-particle tracing model of Na^+ energization on Mercury's dayside. *Journal of Geophysical Research: Space Physics*, 126, e2021JA029587. <https://doi.org/10.1029/2021JA029587>

Received 3 JUN 2021

Accepted 2 OCT 2021

A 3D MHD-Particle Tracing Model of Na^+ Energization on Mercury's Dayside

Austin N. Glass¹ , Jim M. Raines¹ , Xianzhe Jia¹ , Valeriy Tennishev¹ , Yinsi Shou¹, Sae Aizawa² , and James A. Slavin¹ 

¹Department of Climate and Space Sciences and Engineering, University of Michigan, Ann Arbor, MI, USA, ²IRAP, CNRS-UPS-CNES, Toulouse, France

Abstract Data collected by the Fast Imaging Plasma Spectrometer (FIPS) aboard the MEXICO Surface, Space ENvironment, GEOchemistry, and Ranging (MESSENGER) spacecraft showed singly charged Na^+ -group ions at energies of between 1 and 13 keV in Mercury's northern planetary cusp. Most of these ions are likely formed by either photoionization or charge exchange of exospheric Na atoms, with initial energies of approximately 1 eV or less. FIPS observations did not establish which acceleration mechanism most reasonably accounts for this energy gain. Using the Adaptive Mesh Particle Simulator (AMPS) model, we undertake kinetic simulations of 1 eV Na^+ test particles through the electric and magnetic fields output from the Block Adaptive Tree Solar wind Roe-type Upwind Scheme (BATSURUS) global magnetohydrodynamic (MHD) model of Mercury's magnetosphere, in search of plausible explanations for the source of this energization. We find that Na^+ with initial energy of 1 eV are readily picked up by the Dungey cycle return flow in the dayside magnetosphere. In some cases, this flow provides the energy for the ions to escape into the magnetosheath, and in other cases it energizes the ions to hundreds of eV before they pass immediately into the cusp. Those that escape can be rapidly picked up into the magnetosheath flow, where they are accelerated by pickup again up to tens of keV. These one- and two-stage pickup processes on Mercury's dayside can account for the energies of many of the Na^+ ions observed in Mercury's northern magnetospheric cusp by MESSENGER.

Plain Language Summary Data collected in orbit at Mercury showed sodium ions in the northern planetary cusp at high energies. The processes that likely create these ions are only responsible for 0.01%–0.1% of that high energy, and no mechanism previously known to operate at Mercury can account for the difference. We model the Mercury system, and the paths of ions through that system, in search of such a mechanism. We find two mechanisms, both involving energization into proton flows, that explain the data observations.

1. Introduction

Mercury has been a target of interest and study since the flybys by Mariner 10 in 1974 and 1975 and has been subject to intense subsequent study by the MEXICO Surface, Space ENvironment, GEOchemistry, and Ranging (MESSENGER) spacecraft (Solomon et al., 2007), which orbited Mercury from 2011 until early 2015. As many previous works have noted, Mercury occupies a unique place among the solar system's planets. It is situated closest to the Sun, in a plasma and magnetic environment that is an order of magnitude more intense than at Earth and more than 2 orders of magnitude more intense than Jupiter on average (Slavin & Holzer, 1981). As a result, although Mercury has an Earth-like intrinsic dipolar magnetic field and a magnetosphere that obeys the Dungey cycle, its response to external solar forcing is far more dynamic and rapid than is observed at Earth—the reconfiguration time of Mercury's magnetosphere is approximately 2 min, compared to approximately 1 h at Earth (Dungey, 1961; Siscoe et al., 1975; Slavin et al., 2009).

At both Earth and Mercury, the planetary cusps are a key region of the dayside magnetosphere. The cusps of both planets are defined as the region at and above the planetary surface (at Mercury, with its lack of ionosphere) or atmosphere (at Earth) colocated with the foot points of field lines that have just undergone reconnection on the dayside (Cowley & Owen, 1989). These field lines convect through the cusp toward the magnetotail, carrying magnetic and plasma flux as they move (Dungey, 1961). Crucially, these field lines

serve to guide solar wind plasma toward the atmosphere, in Earth's case (Newell & Meng, 1988), and the surface, in Mercury's case (Kallio & Janhunen, 2003).

Understanding the planetary cusps, composed of newly reconnected field lines on which the plasma has direct access to the surface, is crucial for understanding interactions between neutrals in the atmosphere/exosphere and on the surface with the local plasma environment. At Earth, the solar wind has unparalleled access to the neutral atmosphere through the cusps (Smith & Lockwood, 1996). Similarly, Mercury's cusps provide an access route for plasma, including protons and heavier ions, to impinge directly on the planet's surface. This cusp precipitation at Mercury has important implications for exosphere generation, as demonstrated in modeling (Kallio & Janhunen, 2003) and suggested by data (Zurbuchen et al., 2011).

In addition to solar wind plasma, data collected at Mercury show that heavy ions with energies above 1 keV are present a majority of the time in the northern planetary cusp. The Fast Imaging Plasma Spectrometer (FIPS; Andrews et al., 2007; Zurbuchen et al., 1998) instrument flew aboard MESSENGER for its 4-year mission at Mercury. That instrument measured, in part, Na⁺-group ions (a combination of Na⁺, Mg⁺, and Si⁺) with mass per charge of approximately 21–30 amu/e (Zurbuchen et al., 2011). Data collected by that instrument have shown enhancements in these and other planetary ions in Mercury's cusp and that these ions are far more energetic than the processes generating them might suggest (Raines et al., 2014). In particular, those authors report that Na⁺-group ions reach energies of up to 13 keV and that ions in this energy range in the cusp have significant perpendicular velocity components. In analyzing those ions, this work also makes use of data collected by MESSENGER/MAG, a boom-mounted fluxgate magnetometer which collected 20 magnetic field vectors per second at a resolution of 0.047 nT (Anderson et al., 2007).

The most likely generation processes for singly charged heavy ions in the near-Mercury space environment are photoionization, charge exchange, electron-stimulated desorption, sputtering, and micrometeoroid vaporization. Some previous work in exosphere modeling assumes that sputtering and electron-stimulated desorption produce ions at the same energies as photoionization (Cassidy & Johnson, 2005). Other work assumes that losses of exospheric neutral Na particles due to photoionization are large relative to these other processes (Leblanc & Johnson, 2003). As either approach produces the same outcome for our simulation, we follow their lead and exclude consideration of processes other than photoionization, insofar as they would result in ions of significantly less than 1 eV, or ions generated on the nightside. That the typical expected energy of newly generated Na⁺ is approximately 1 eV means that the observations documented in Raines et al. (2014) of hundreds of eV to keV Na⁺-group ions in Mercury's northern cusp and dayside is an enigma. This work seeks to resolve that enigma and provide a plausible explanation for Na⁺ acceleration on Mercury's dayside.

Raines et al. (2014) suggested three primary means by which Na⁺-group ions might be energized from the eV energies at which they are generated up to the keV energies at which they are observed in the cusp and across the dayside. The first suggestion is that these ions are generated in or near the cusp and accelerated by local processes, and the second is that these ions have been drawn into the reconnection region and accelerated, and then subsequently swept into the cusp. They note that, of these two explanations, the latter more readily explains the presence of energized Na⁺-group ions observed in Mercury's northern cusp. The third suggestion is that neutral Na atoms of planetary origin may have traveled into the magnetosheath or even the solar wind, been photoionized there, and then accelerated via pickup into the magnetosheath flow before passing into the cusp. The amount of energy gained in such a process, as is noted, depends on the convective electric field, itself a product of the local plasma flow velocity and the magnetic field (Möbius et al., 1985). Finally, it is also possible that ions are energized in the tail and then return to the dayside and the cusp. The theoretical maximum energy that an ion could obtain moving across the tail through is set by the cross-magnetospheric electric potential. This potential was estimated at Mercury using MESSENGER flyby data in Slavin et al. (2009) as approximately 30 kV. This estimate has most recently been refined by Jasinski et al. (2017), who estimate the average cross-magnetospheric potential to be approximately 19 kV, though with significant variation between 1 and 74 kV.

We undertake modeling of Na⁺ on Mercury's dayside in search of a plausible explanation for the keV ions observed by FIPS from among these and any others captured by our approach. The application of our methodology to modeling sodium ions at Mercury is not completely new; however, our work is uniquely

designed to address sodium energization into the cusp by our model's inclusion of a conducting core layer, by our model's creation of a highly realistic magnetosphere including realistic locations for the cusp and dayside closed field regions in simulation output (Jia et al., 2015), and by our focus on the energization of ions ultimately passing through the cusp, rather than those residing in or near the equatorial plane. Our work follows a number of other studies modeling particle energization in Mercury's magnetosphere in the last two decades, including modeling of centrifugal energization of Na^+ and other planetary ions on Mercury's nightside (Delcourt et al., 2002, 2003), modeling of electron dynamics during substorm dipolarization (Delcourt et al., 2005), a characterization of centrifugally stimulated exospheric escape of Na^+ ions into the magnetosphere (Delcourt et al., 2012), and an investigation into a high energy sodium ring (Yagi et al., 2017). The deeper understanding of Na^+ energization specifically on Mercury's dayside into the cusps that this work seeks to produce will allow comparison with data having been and soon-to-be collected in those regions and, like previous work, will inform the anticipated effectiveness of Na^+ precipitation as a source for atoms in Mercury's exosphere.

This manuscript proceeds first with a discussion of our approach to modeling the energization of Na^+ ions with a particle tracing model through magnetohydrodynamic (MHD) fields. Then, we briefly examine the statistical output of this modeling by identifying three typical trajectories that Na^+ ions follow in our simulation before passing through the northern cusp. We examine two of these trajectory types in detail with two representative time series, explaining the energization mechanisms at play in both. We close with a visualization of the 3D velocity distribution of one of these trajectory types at various key points in space, and a discussion of the potential uses and limitations of our work.

2. Methodology

2.1. Models

Our analysis makes use of two well-established models, Block Adaptive Tree Solar wind Roe-type Upwind Scheme (BATSRUS) and Adaptive Mesh Particle Simulator (AMPS). The BATSRUS model is a global MHD model designed to simulate the space environment of a magnetized or unmagnetized planetary body by solving the MHD equations with a conservative finite-volume method over an adaptive simulation domain (Gombosi et al., 2002; Powell et al., 1999). BATSRUS has been developed and used for over 20 years to model Earth's space environment (Tóth et al., 2012), and it is the global MHD model used within the Space Weather Modeling Framework (SWMF), which couples models with highly varied physics and scales. BATSRUS has previously been successfully applied to various planets other than Earth as well, such as Mars (Ma et al., 2002; Najib et al., 2011), Jupiter (Sarkango et al., 2019), and Saturn (Jia, Hansen, et al., 2012; Jia, Kivelson, et al., 2012).

BATSRUS has also been successfully applied to modeling of Mercury's space environment (Jia et al., 2015, 2019)—the simulations used in our analysis are taken and derived directly from that work. They feature a nonuniform spherical grid, in which the resolution of each grid cell, measuring approximately the distance between opposite corners, ranges from 20 km near the surface to 50 km near $2 R_M$ (where R_M means, Mercury's average radius, about 2,440 km). Importantly, the implementation of BATSRUS presented in that work and used in this study includes Mercury's core induction effect, by treating the top layer of the core as a region of finite conductivity, thereby permitting induced currents. Mercury's induction effect is the process by which changes in the solar wind conditions drive induction currents on the surface of the core, generating magnetic field that enhances the dipole field and opposes the solar wind changes (Slavin et al., 2014). Modeling this effect enables a more realistic model of the planetary response to solar wind forcing and allows the model to generate a highly realistic magnetosphere and plasma environment, as demonstrated by the model-data comparisons shown in previously published model results (Jia et al., 2015).

The AMPS model traces particles according to simple force laws through the near-space regions of various planetary bodies, including planets, planetary moons, and comets (Tenishev et al., 2021). AMPS is a numerical kinetic model designed in a direct simulation Monte Carlo style, which solves the Boltzmann equation for a one-particle distribution function for each particle simulated. In AMPS, many particles are simultaneously simulated on a set of meshes with different levels of grid refinement. The simulation begins from an initial coarse grid and refines as necessary until steady state convergence is established. The output of such

Table 1
MHD Simulation Parameters

	“Idealized” set	“M2” set
IMF (nT, MSO)	<0, 0, -20>	<-15.2, 8.4, -8.5>
SW velocity (km/s, MSO)	<-400, 0, 0>	<-400, 50, 0>
SW proton density (per cm ³)	40	40

a simulation permits not only analysis of the steady state solution but also analysis of the dynamics of the system, by evaluation of the trajectories of each ion at any point in time.

AMPS was initially developed and implemented to model the multispecies cometary coma of 67P/Churyumov-Gerasimenko, visited by the Rosetta spacecraft. It has been successfully applied to studies of that comet both before and since the rendezvous with Rosetta (Fougere et al., 2016; Tenishev et al., 2008). Like BATSRUS, AMPS has also been applied to Mercury’s space environment, as reported by Tenishev et al. (2013). In

this study, we do not make use of the capabilities of AMPS to model Mercury’s neutral exosphere nor particle-particle collisions.

Both BATSRUS and AMPS have adaptive capabilities; based on certain key parameters, the models will automatically refine the simulation domain to ensure sufficient detail is resolved. In our implementation, the BATSRUS model performs adaptive refinement of the simulation domain. Although AMPS does not perform automatic refinement of the simulation domain, because the BATSRUS fields form the basis for the forces in the AMPS model the refinement is carried over from the MHD run to the kinetic simulation.

The resolution of the AMPS domain is 80 km between the surface and $2 R_M$ and then relaxes to larger values outside that threshold. Although $2 R_M$ would be quite close to the surface for some applications, MESSENGER data demonstrated that the magnetopause standoff distance at the subsolar point is, on average, $1.3\text{--}1.4 R_M$ (DiBraccio et al., 2013; Slavin et al., 2010; Winslow et al., 2013). We therefore believe $2 R_M$ is an appropriate choice for the outer boundary of our fine-resolution grid, for a study of this level of specificity. Mercury’s near-space environment is noncollisional, and our model does not seek to resolve the ionization processes themselves. Therefore, the scale lengths for collisions and the various ionization processes are not the most relevant factors for consideration when choosing the grid resolution. Instead, the appropriate scale length for our particle tracing is the ion gyroradius, as ion gyromotion is the smallest motion we seek to resolve in this study. For the ions in our simulation, sodium ion gyroradius is smallest in the dayside closed field region. In this region, the magnetic field strength is on the order of 100 nT and the perpendicular speed of the Dungey cycle return flow that feeds directly into dayside reconnection typically ranges between a few kilometers per second up to about 50 km/s. In this environment, the vast majority of sodium ions achieve a perpendicular velocity of only 20 km/s within a fraction of a second of their generation. A sodium ion with this perpendicular velocity has a gyroradius larger than 80 km, making 80 km a sufficient choice for our study. The only error resulting from this choice occurs in the very beginning portion of a small fraction of ion trajectories, before they attain tens of km/s of speed. However, because these ions do not move significantly from their start locations before achieving this speed, and because we are not attempting a simultaneous time-accurate simulation of their trajectories, this error should not affect our results as long as we begin our analysis after this point in the trajectories, which we do. Nonetheless, we tag these ions separately in the proceeding analysis.

We use two sets of MHD fields output as input to AMPS: the set reported in Jia et al. (2015) and another produced through the same means with idealized upstream conditions. The previously published results used in this analysis were produced through modeling the second flyby of Mercury by MESSENGER (“M2”). Upstream conditions for this run, and for the idealized upstream condition run, are represented in Table 1. The IMF (interplanetary magnetic field) direction and solar wind velocity are presented in Mercury solar orbital (MSO) coordinates, in which the X coordinate is positive in the direction of the Sun, Z is positive in the northward direction, and Y completes the right-handed coordinate system (pointing duskward from the origin at the center of the planet).

We choose to approximate the geometric locations for the northern and southern cusps in the MHD output produced through the two fields sets as rotated rectangular prisms. Although it would have been theoretically possible to identify the cusps using a more rigorous numerical method, such as outlining the region using a set of selection criteria based on magnetic field topology and plasma pressure and density, this would have been an exponential increase in complexity without justification in our approach. Because we are comparing our results to observations by a single spacecraft and only searching for plausible explanations

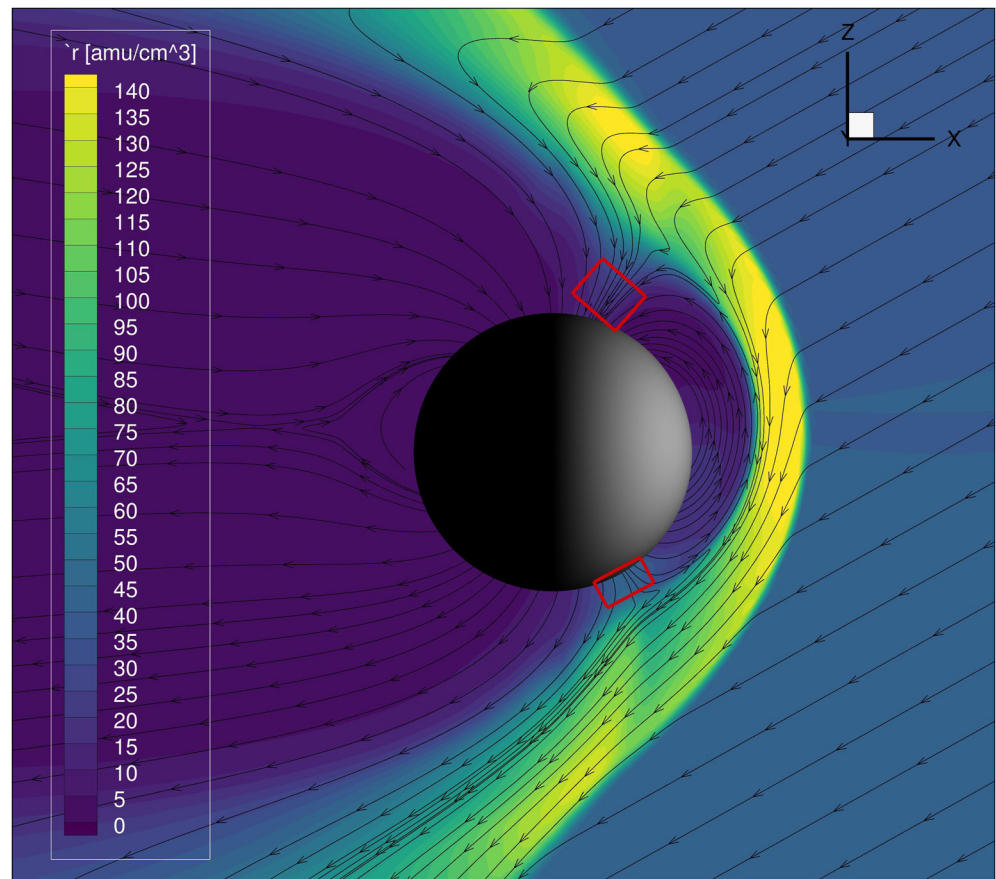


Figure 1. Cusp locations in X - Z plane of M2 fields output as red boxes. Background flooded according to proton density, with flow lines of magnetic field in the plane. The magnetopause can be clearly seen in both background flood and magnetic field flow lines, as the boundary between higher and lower plasma.

for ion acceleration, simply identifying ions in the vicinity of the dynamic cusp region, and evaluating the processes by which they were accelerated, should be sufficient to address our needs.

The cusp regions are identified in the MHD output where pressure and density are high compared to the dayside closed field region. First, an X - Z cross section of the MHD output data is examined by eye. An X - Z coordinate sitting along the first reconnected field line becomes the sunward edge of the cusp box. Then, the tailward edge of the cusp box is identified in the same view by selecting an X - Z coordinate along an unlinked field line (part of the lobe) which matches the density of the point selected for the sunward edge. For the northern cusp, this value is approximately 8.5 amu/cm^3 , and for the southern cusp approximately 35 amu/cm^3 . The asymmetry between the northern and southern cusp definitions arises because Mercury's magnetic field is best modeled as a dipole offset to the north by 20% of the planet's radius (Anderson et al., 2011). The remaining two edges perpendicular to the X - Z plane are determined by rotating the two edges already selected until the resulting box approximately overlays the region in which density is higher than 8.5 and 35 amu/cm^3 , respectively. The y extent of each cusp is $0.82 R_M$, an approximate size chosen to cover a significant extent of the sunward face of the planet but stopping short of including regions of the sheath at the flank that would confound any statistical results. Figure 1 shows a projection of the MHD output on the X - Z MSO plane, with our identified cusps appearing as red boxes. Although Figure 1 shows the M2 fields case, the cusp locations are identical in the idealized fields case.

2.2. Simulation

In order to examine the trajectories of 1 eV sodium ions on the dayside, we performed a simulation of the flight paths of 500,000 sodium ions through each of the two sets of MHD fields described above. These ions are generated within our simulation domain distributed uniformly across 6–18 h local time, across all latitudes except those within 20° of the north pole (to the exclusion of latitudes that would have placed particles within the northern cusp at start), and from 1.01 to 1.6 R_M altitude. In Figure 1, the outer extent of this source volume extends about one third of the way into the green-yellow region of high density at the subsolar point, above the magnetopause. These ions are generated with a random velocity vector direction and 1 eV of kinetic energy.

Although not presented here, sensitivity analyses performed with as few as 10,000 particles do not produce drastically different results to our 500,000 particle simulations—such analyses still show each of the major ion types we have identified here. We therefore find that 500,000 particles is a satisfactory trade-off between beneficial and useful statistics, and the amount of time it takes to run and postprocess. On a massively parallel supercomputer, the trade-off particle number would be far higher and permit analyzing less common phenomena.

Although it would be surprising to discover that the density of sodium over this region was uniform, we believe a weighting which gives each possible start location equal likelihood to be the origin of cusp sodium is most appropriate for the goals of this study. A uniform distribution in space provides the highest probability that we will simulate all possible sodium ion trajectories which pass through the northern cusp.

In AMPS, ions move according to the terms of the Lorentz force, where the particle velocity vector is tracked by AMPS and the magnetic field is generated with BATSRUS. In simulation, the electric field is purely the convective electric field of the background proton plasma, obtained in space with $\vec{E} = -\vec{U} \times \vec{B}$, where \vec{U} is the flow vector of the background plasma from MHD. Na^+ trajectories are sampled at a constant time rate which is allowed to freely vary from particle to particle. For 97.5% of particles, the chosen time step is ~ 0.16 s, and in no instance is it greater than 1 s. The gyroperiod of a sodium ion in a 250 nT magnetic field, approximately the strongest field experienced in our simulation, is approximately 6 s, much larger than our time step. Each particle is propagated through the modeled fields until it leaves the simulation domain, either by impacting the surface or by escaping the system by arrival at the outward extent of the simulation box. Upon completion of the simulation, we evaluate the trajectory data. Through simple geometry, we first document where along each particle's trajectory it passes through the cusp, if at all. For data management purposes, the trajectories of all particles which do not traverse the cusp are not subject to further analysis.

From this reduced data set, we perform a categorization of the ions based on aspects of their trajectory which we anticipate will inform the controlling energization mechanism. We first classify as “Type 0” any ion which experiences a background plasma density of greater than 50 amu/cm^3 prior to traversing the northern cusp, a clear indicator that the ion passes through the magnetosheath prior to cusp traversal. We classify as “Type 1” any particle which does not pass through a region where the density is greater than 20 amu/cm^3 (i.e., any particle which is generated in the closed field region on the dayside and moves from there to the cusp without crossing or coming near the magnetopause). We classify as “Type 3” any ion which crosses a region where the background density is greater than 20 amu/cm^3 but less than 50 amu/cm^3 ; this rare typing represents ions which come close to crossing the magnetopause into the sheath but do not clearly do so. From these top-level classifications, we subcategorize Type 1 ions into Type “1a” and “1b” ions, depending on whether it takes fewer or greater than five simulation time steps (less than 1 s each, as described above) for the ion to begin to be picked up into the dayside Dungey cycle return flow, respectively. Type 1b ions are those flagged as having a potentially erroneous beginning portion of their trajectories, due to the limits of the resolution of our simulation domain as described above. However, after they achieve tens of km/s of speed, they are indistinguishable from their Type 1a relatives, and we analyze them from there. Finally, given that the grid resolution in our model becomes relatively coarse above 2 R_M , we group any ion of any other type which exceeds a radial distance of 2 R_M before traversing the cusp into “Type 2.” The results of this classification scheme can be visualized in the pie graphs in Figure 2.

Although the total number of ions passing through the cusp is a low fraction of the million particles, any analysis of the fraction of ions passing through the cusp among those generated will not be physically

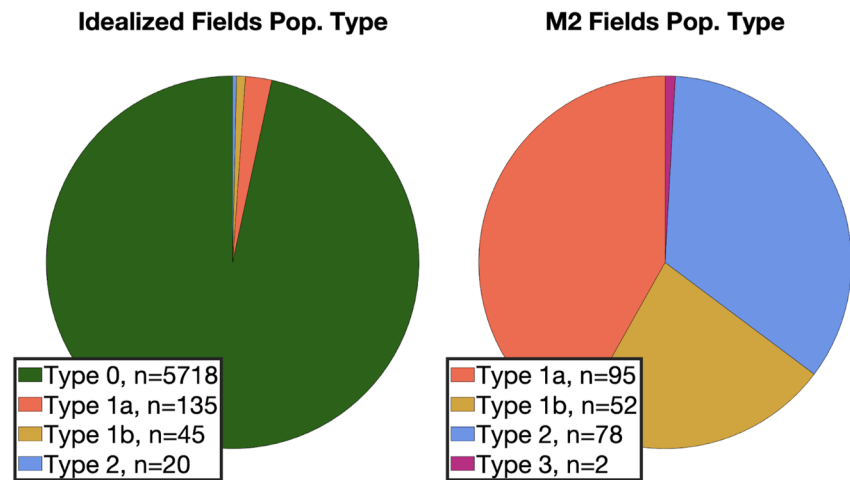


Figure 2. Pie graphs of ion type in each of our two simulations. The relative abundance of Type 0 ions in the idealized fields case, and of Type 1 ions in the M2 case, is notable.

meaningful, because of the nonphysical source volume used in the model. A physical source volume would have required a realistic exosphere model from which to derive photoions; although such an approach would have allowed for a more rigorous quantitative comparison to data, it would not have been the most computationally efficient way to address the simpler question of what energization mechanisms operate at Mercury that can account for Na^+ energy gain. Instead of generating ions from a realistic exosphere, for the purposes of this study, we believe it is best to perform comparisons of the relative abundance of different ion types within each run. This approach is especially helpful in determining times when different upstream conditions cause energization to dominate in different regions of the dayside and sheds light on the dayside volume that is most likely to produce ions observed with keV energies in the cusp.

As demonstrated by the ion counts in the legends of these graphs, Type 0 particles are substantially more abundant than other types when the field configuration accommodates them, such as in the idealized fields case where they are over 96% of simulated cusp ions. However, Type 1 particles are the dominant particle type in the more magnetically complex M2 fields case, where they make up approximately 65% of simulated cusp ions.

A sample trajectory of one of the Type 0 particles from the idealized simulation is plotted in Figure 3. From top to bottom on the left-hand side, the panels show the particle's energy, the magnitude of the perpendicular component of the background plasma flow speed, the magnitude of the magnetic field, the magnitude of the electric field, and the particle's altitude. These variables are plotted against the time since the particle generation on the X axis. The two panels on the right-hand side show a 3D view of the particle's trajectory, projected into the MSO X - Z and X - Y planes. The red boxes in the right panels show the cusp locations, also shown in outline in Figure 1. The light blue outline shows the approximate magnetopause surface, modeled according to Shue et al. (1997) as previously successfully applied to Mercury's magnetopause by DiBraccio et al. (2013). The black line shows the particle's trajectory and is labeled with letters A–E, matching the vertical dashed lines at left, at important locations in the particle's trajectory.

This particle begins its trajectory in the closed field region, distinguishable by examination of the trajectory in the right projections, and the panels showing flow speed and magnetic field at point A on the left. From its generation, while still inside the closed field region before point B, it quickly gains 3 orders of magnitude of energy. As the energy panel at left demonstrates, the particle performs two full gyrations in the closed field region—the particle gyrates perpendicular to the magnetic field as it drifts through the closed field region, tracing either a cycloid or prolate cycloid (i.e., without or with smaller loops); along this path, the particle's energy fluctuates between a low and high point, exactly as depicted in the top panel. In its approach to and through the magnetopause from approximately 12 s to point B, the particle undergoes approximately an order of magnitude of energization, from hundreds of eV to 1 keV of energy. After it crosses the magnetopause at point B, the particle travels within the magnetosheath, evident in its trajectory in the right-hand

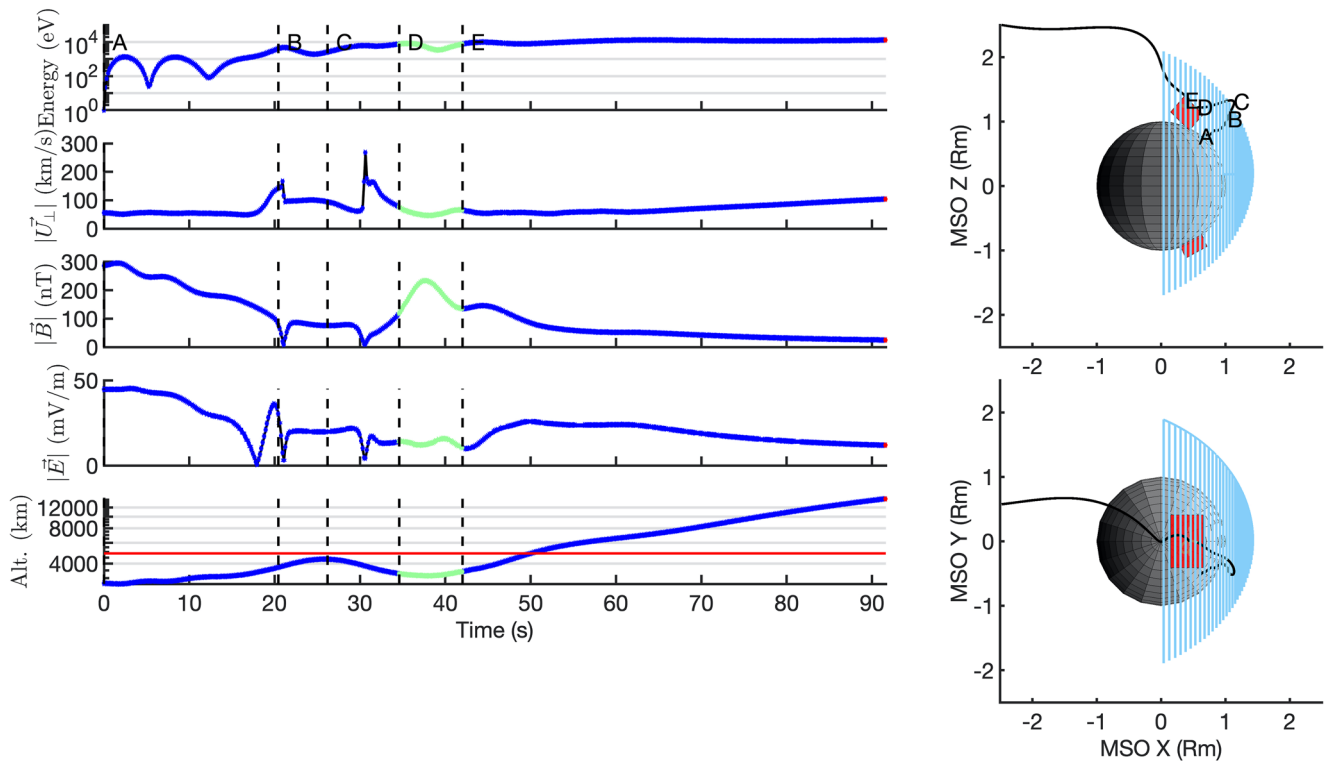


Figure 3. Trajectory overview plot for a typical Type 0 ion from the idealized fields set. At left, panels showing particle energy, plasma perpendicular flow speed, magnetic field strength, electric field strength, and particle altitude, with a red line plotted at $2 R_M$, the upper limit of the refined region of our simulation. All are plotted against time since particle generation on the horizontal axis. At right, 2D projections of the particle's 3D trajectory, with modeled magnetopause and imposed cusp boxes plotted for reference.

trajectory diagrams. During its magnetosheath crossing, centered on point C, the particle's energy increases to nearly 10 keV, after which it passes back through the magnetopause at time 30 s, and into the cusp at point D. The particle experiences a small energy fluctuation in the cusp, colored green in the left panels, before exiting at point E at nearly the same energy it entered with. Our analysis is no longer robust shortly after this point when the particle's altitude exceeds the red $2 R_M$ line in the altitude panel and enters the coarsely refined portion of our simulation domain.

It is typical for Type 0 particles to traverse the magnetosheath more than once; although the majority of particles in our simulation (approximately 51.5%) only cross through the magnetosheath once, nearly 30% do so twice, 13.5% do so 3 times, 4% do so 4 times, and the remaining 1% of particles do so 5–8 times. Although these ions start in somewhat different positions on the dayside in the prenoon sector, just as in Figure 3, each of them is accelerated such that it gyrates out of the closed field region, is energized in the magnetosheath, and passes through the northern cusp before flowing down the magnetotail.

A sample trajectory of one of the modeled Type 1a ions is shown in Figure 4 in the same style as its Type 0 counterpart. In contrast with the Type 0 ion, the Type 1 ion is characterized by the fact that it does not leave the closed field region before crossing through the northern cusp. Instead, as demonstrated in its trajectory in Figure 4, this type of ion moves from its generation location immediately to the cusp. In additional contrast to Type 0 ions, it is noteworthy that Type 1 ions do not bounce in the cusp—instead, they simply graze the cusp at a high altitude, passing through it as they flow down the magnetotail. Despite the fact that they skim the cusp, rather than bounce within it, their presence in this location in space means ions with such trajectories would have been observable by the FIPS instrument; thus, they are an important part of our analysis.

That these Type 1 ions merely skim the cusp suggests our choice of cusp location, discussed in relation to Figure 1, may have a significant influence on the outcome of our simulation, and in particular on the

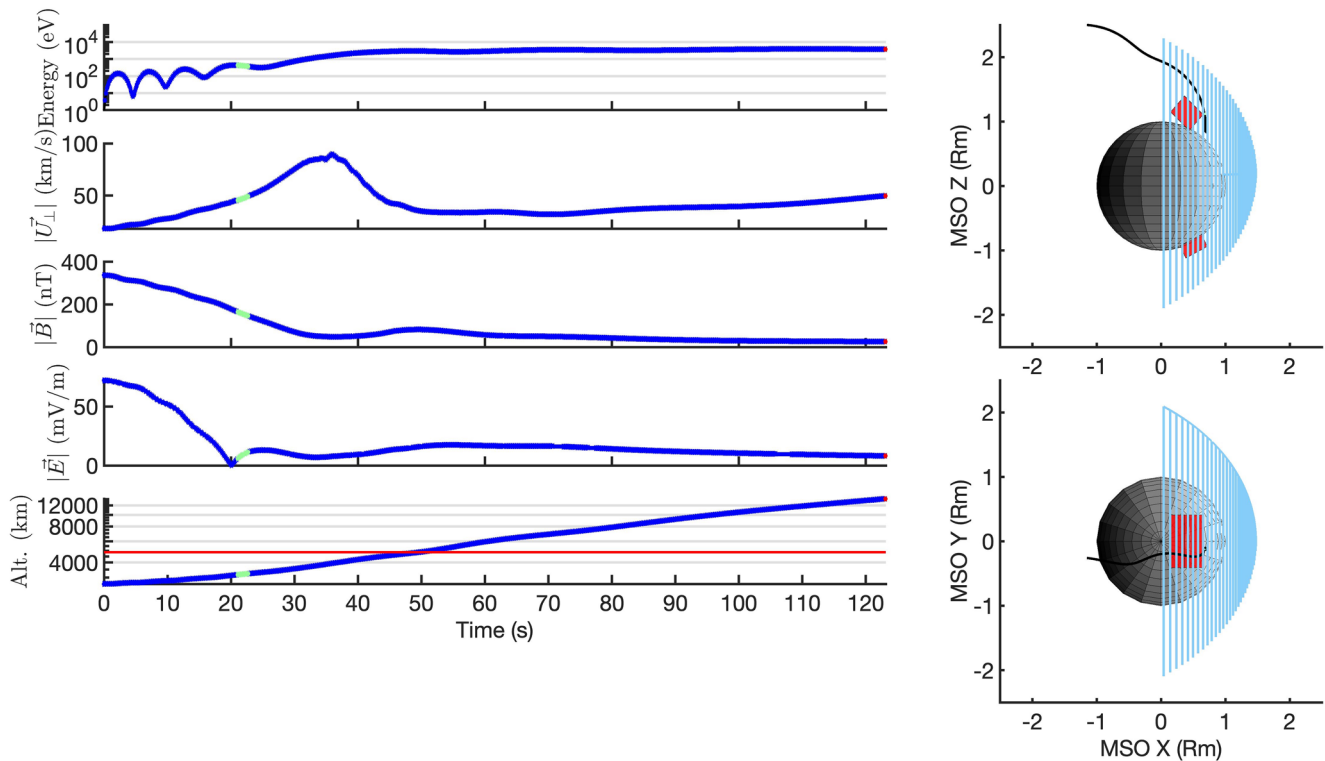


Figure 4. Trajectory overview plot for a typical Type 1 ion, which appears in both the idealized and M2 fields sets, in the style of Figure 3. This specific particle was taken from the M2 fields output.

absolute quantity and relative abundance of the two major ion types we identify. For Figure 1 and the ensuing analysis, we chose the radial extent of the northern cusp bounding box conservatively, to ensure that our comparison with data was faithful to the portion of the modeled region that FIPS-MESSENGER would have traversed. However, given the possibility that our chosen cusp box might not extend far enough in the radial direction to capture some number of Type 1 ions grazing the cusp box, we undertake a simple

sensitivity analysis, increasing by 50% the length of the two cusp box faces aligned most closely with the radial direction. Conducting the same analysis that produced Figure 2, we find that, in this expanded cusp box simulation, the number of cusp ions is multiplied by 2X in the idealized fields case and by over 5X in the M2 fields case. However, increasing the cusp box length does not result in the observation of any Type 0 ions in the M2 fields case, and only increases the relative abundances of Type 1 ions to Type 0 ions in the idealized fields case from approximately 2% to approximately 7%, meaning Type 0 ions continue to be far and away the dominant population in that configuration. Because our analysis does not rely on the absolute number of cusp ions, and because the relative abundance was not significantly affected by the 50% increase in cusp size, we are confident that our work is sufficiently insensitive to our chosen cusp boundaries. Versions of Figures 3 and 4 showing components of the velocity and magnetic field can be found in Supporting Information S1.

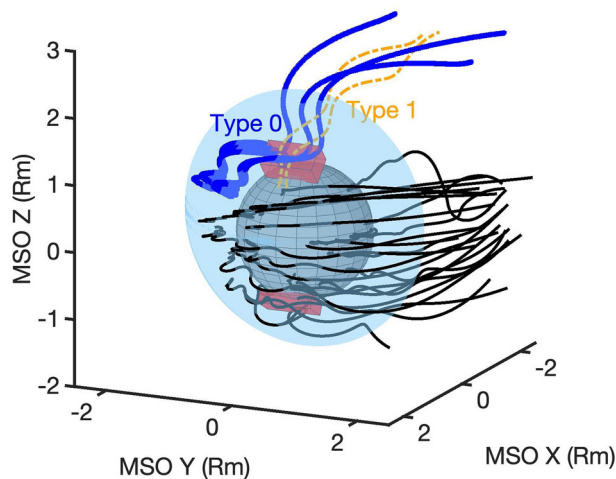


Figure 5. A global view of sample ion trajectories from simulation output. Blue thick trajectories are Type 0 ions, dashed orange trajectories are Type 1 ions, and black trajectories are a sampling of the remaining 99% of ions in our simulations. The light blue surface represents the magnetopause, as in Figures 3 and 4.

Figure 5 provides a summary of the output of our simulations. Just as in the two trajectories on the right sides of Figures 3 and 4, we have plotted a 3D visualization of Mercury in the MSO coordinate system, our definitions of its cusps in red, and a modeled magnetopause surface in light blue. We have added to this visualization three groups of ions: a group of ions in thick blue exiting the closed field region and then reentering

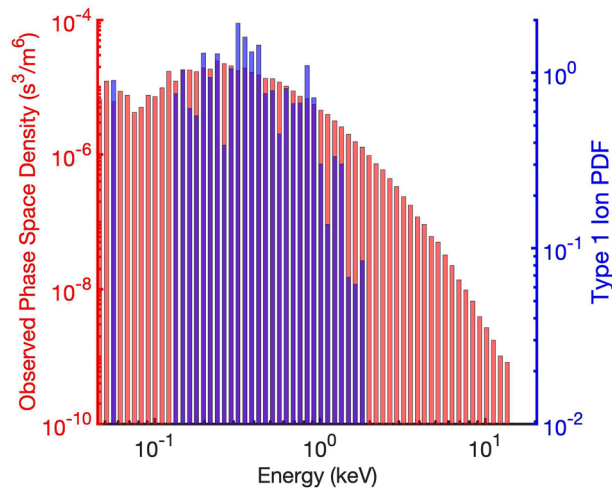


Figure 6. Data and Type 1 modeled ion energy. The left y axis (red) shows mission-averaged Na^+ phase space density (in s^3/m^6) in the northern cusp observed by MESSENGER. The right y axis shows a probability density function (PDF) of Type 1 ions across the Fast Imaging Plasma Spectrometer (FIPS) energy bins, across both simulations, immediately after they enter the cusp.

it before crossing through the cusp, representing Type 0 ions; a group of ions in dashed orange that flow directly from their start location to the cusp, representing Type 1 ions; and an unlabeled ion group in black flowing out into the sheath, joining the flow around the planet and down the magnetotail.

This latter group in black represents the behavior of over 99% of the noncusp ions in our simulations, which almost exclusively flow to the nightside and down the magnetotail immediately after crossing into the sheath. This dawn–dusk asymmetry in ion trajectory is a consequence of effects of the convective electric field in the closed field region and in the magnetosheath, which may differ based on the IMF direction. Our simulation has demonstrated that the motion of Na^+ on the dayside is nonadiabatic, dominated at different points along an ion's trajectory by gyromotion and by guiding center drift. Ions generated on the dusk side are very likely to gyrate into the magnetosheath and be carried down the magnetotail on that side of the planet. Ions generated on the dawn side, in contrast, begin their trajectories by drifting toward the subsolar point within the closed field region. At some point, each such ion gyrates out into the magnetosheath, where its motion is controlled by gyration. It performs a half gyration in the magnetosheath, moving toward dusk, and then returns to the closed field region, where it performs another half gyration which is also oriented toward dusk because the field is oppositely oriented to that in the magnetosheath. In this way, by a combination of

gyromotion and guiding center drift, even ions initialized on the dawn side are ultimately picked up into the magnetosheath flow on the dusk side and move down the magnetotail and out of the simulation, giving rise to the asymmetry observable in Figure 5. A small minority of the ions which do not traverse the cusp follow more complex trajectories before flowing down the magnetotail, however, those trajectories cross into the coarsely resolved region of our simulations. Because of this, and since ions which do not cross through the cusp are not the subject of this study, we do not investigate them further.

3. Results: Energization in the Dayside Magnetosphere

3.1. One-Stage Energization

Through statistical examination of the trajectories of both Type 0 and Type 1 ions using the quantities displayed in Figures 3 and 4, we develop the first important conclusion of our work—sodium ions born in the closed field region which ultimately pass through the cusp are rapidly picked up into the return flow of the dayside closed field region.

The most common population type in the M2 simulation is Type 1 ions, those which are generated in the closed field region and move directly from there to the cusp without crossing the magnetopause. It is relevant to note here that although Mercury lacks a collisional atmosphere, its dayside magnetosphere is not devoid of plasma. Instead, the dominant population in this region is likely sunward-flowing plasma returning magnetic flux from the night side in completion of the magnetospheric Dungey cycle (Dungey, 1961; Slavin et al., 2010). In both of our MHD model outputs, we find a typical perpendicular flow speed on the scale of 50 km/s in this region. Left panel 2 of Figure 3 shows a perpendicular flow speed of almost exactly 50 km/s at that ion's starting latitude and altitude.

Recalling that all of the particles in our simulation begin at 1 eV, we establish a scale for the energization of ions in our simulation by examining the energy of Type 1 ions at the first point along their trajectory during which they are in the cusp. A visualization of this examination is shown in Figure 6.

In Figure 6, we compare a probability density function of the energies of Type 1 ions from both fields sets upon arrival at the cusp with the MESSENGER mission-averaged phase space density distribution of sodium ions, treating every FIPS sodium collection in the northern cusp as part of a single distribution. As a caveat, note that this figure and the other like it do not take into account the limited field-of-view of the FIPS

instrument. As FIPS did not produce a complete profile of Na^+ in 3D velocity space, the data distribution on the red left Y axis should not be understood as a complete observation of Na^+ in the northern cusp. It is very possible, especially given the nonisotropic nature of Na^+ that we observe in simulation output, that there are trajectories which FIPS does not observe and are not reflected in those figures. Our analysis only seeks to provide plausible explanations for the energies of ions that FIPS did observe.

For ease of comparison, we histogram the simulation output on the right Y axis according to FIPS energy bins. Although the statistics on Type 1 ions are somewhat low, the average energy and distribution shape clearly compare as similar to the FIPS data in the relevant range for Type 1 ions. Thus, we find that the Type 1 energization mechanism in our model, which accounts only for energization resulting from the convective electric field, can fully account for the energy of the average Na^+ ion observed by FIPS in the cusp. We therefore conclude that pickup resulting from the convective electric field in the dayside closed field region, sourced from the Dungey cycle return flow in this region, provides a plausible explanation for the energy of the average Na^+ ion in Mercury's northern cusp.

3.2. Two-Stage Energization

In Earth's magnetosphere, heavy ions like O^+ have predominantly planetary origins. These heavy ions are trapped in Earth's closed field region, in the ring current and elsewhere in the plasmasphere. Transport across the terrestrial dayside magnetopause into the magnetosheath is an observed loss mechanism for such ions but is minor compared to the loss rate on the nightside (e.g., Paschalidis et al., 1994). Although we are unable to make an estimate of the importance of loss through the dayside magnetopause at Mercury, we find and will discuss in this section that, in contrast to Earth, it is a dominant process within the confines of our simulation for generating high energy Na^+ ions in the cusp.

Type 0 ions, by far the most abundant in our simulations among ions crossing the northern cusp, are separated from the other types by their traversal of the sheath prior to entering the cusp. As anticipated by Raines et al. (2014), some of the ions in this type generated in the sheath are able to access the northern cusp. The remaining ions of this type, however, are generated within the closed field region on the dayside. Just like the Type 1 ions discussed above, these Type 0 ions are quickly accelerated due to the convective electric field, attaining energies of hundreds of eV in a matter of minutes or less.

The convective electric field is, by definition, perpendicular to the local magnetic field. Thus, in any given time step, the energy imparted by the convective electric field has a significant impact on the gyroradius. When the local field is strong enough and the ion makes sufficient gyrations in the closed field region without colliding with the planet or traveling down the magnetotail through the cusp or flank, the convective electric field increases its gyroradius to greater than the thickness of the magnetopause. With its trajectory no longer bound to follow the closed field lines in the dayside magnetosphere, it is able to cross the magnetopause and escape into the magnetosheath.

Upon crossing into the sheath, Type 0 ions are subjected to a second stage of rapid acceleration. The background flow speed in the sheath varies significantly from near stagnation at the subsolar point to nearly the solar wind speed at the cusp, but the vast majority of ions exiting the magnetosphere into the sheath in our simulation immediately experience plasma flow on the order of hundreds of kilometers per second.

Even for Type 0 ions which spend only minutes in the sheath, there is significant energy available in the magnetosheath flow for energization to the scale observed by FIPS. In the left panel of Figure 7, we see the energy change in a Type 0 ion's first pass through the magnetosheath. This quantity represents different milestones for different particles: for some ions, this range stretches from near its generation point to its passage into the cusp; for others, it represents the energy gained over a fraction of the ion's trajectory, between its residence in the closed field region and its ultimate passage from that region into the cusp; and for yet others, it represents the energy gained from the first one of many passes through the sheath, on its winding trajectory to the cusp. In all cases, however, the distribution establishes that proton flow in the magnetosheath is a significant source of free energy, on the order of keV. Figure 7, right, with the same style as Figure 6, demonstrates the potency of the sheath electric field clearly—Type 0 ions all have 1 keV or more energy by the time they reach the cusp. Given that a singly charged sodium ion fully picked up into

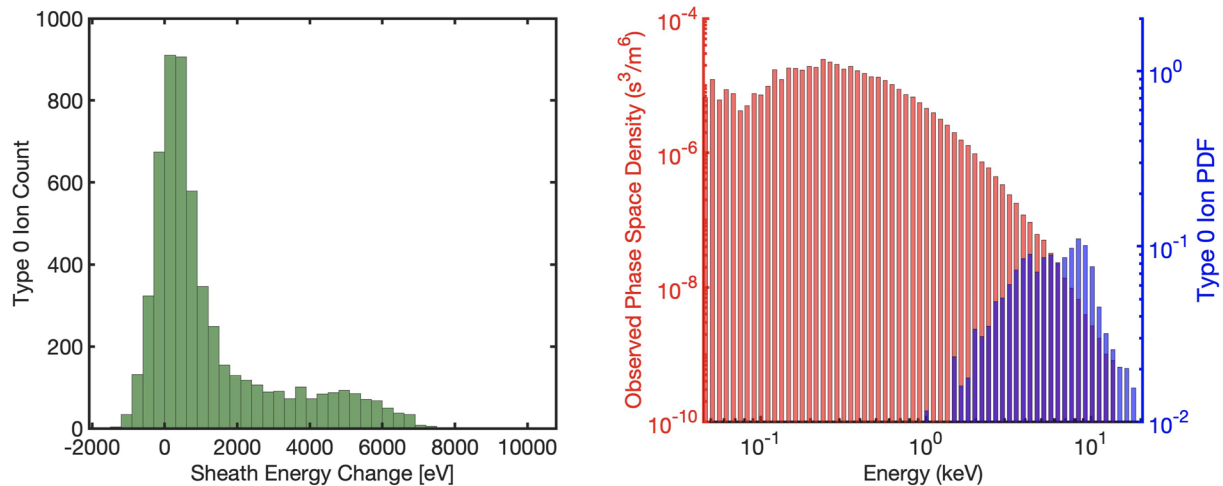


Figure 7. At left, a histogram of the energy change Type 0 ions experience in their first (and only, in some cases) passthrough of the magnetosheath. At right, the cusp energy distribution of Type 0 ions compared with FIPS mission-averaged Na⁺ cusp phase space density, in the style of Figure 6.

a 400 km/s flow would have an energy of approximately 20 keV, the results displayed in Figure 7, right are evidence that the pickup process in the sheath acts quickly and effectively to accelerate Na⁺ ions.

Although this level of energization provides a satisfactory explanation for the higher energy range of ions observed in the cusp not accounted for by Type 1 ions, it is important to note at least two factors that could affect interpretation of the results in both Figures 6 and 7.

Care must be taken when making comparisons of our simulation results to Na⁺-group ion energy distributions accumulated over the entire 4-year MESSENGER mission. First, although comparisons between data and model ion energies are reasonable, because we have designed our modeling approach to search for energization mechanisms in the models that can account for data, it may be inappropriate to compare the mission-averaged phase space density of ions to any one ion type, beyond the order-of-magnitude analysis performed here. The mission-accumulated distribution represents Na⁺ ions over a large range of activity in Mercury's magnetosphere. Given the variability of Mercury's magnetosphere, it is not possible to represent Mercury's dynamic response to its external environment with a single set of upstream conditions. Instead, we chose to model Na⁺ ions in our idealized and M2 fields sets because they are representative examples of idealized and realistic conditions, respectively. As the instantaneous speed of the return flow and sheath flow change with changing external conditions, so too might the average energies and energy distribution of Na⁺ passing through these regions. Over the course of the entire mission, this significant variability in external conditions would thereby become incorporated into the average Na⁺ phase space density distribution in the cusp. Because of sparse data and the lack of an upstream monitor concurrent with FIPS measurements, at this time we feel unable to state with any certainty that these energization mechanisms are conclusively responsible for any portion of the observed energetic sodium ion density.

Second, because we did not assess which of the two sets was more representative of the reality at Mercury, one must be wary of directly comparing the output of our two runs to each other. An unscaled comparison, for example, assumes the same relative frequency of the underlying IMF and solar wind conditions in the long term, and that the generation rate and spatial distribution of Na⁺ under these varied conditions are the same. Neither can be assumed. Instead, we confine ourselves to our energization analysis, which, according to Figures 6 and 7, is sufficient to establish that pickup in the closed field region on the dayside is a significant potential source of energy and that pickup into the sheath can explain even the highest energy cusp sodium observations under typical upstream conditions.

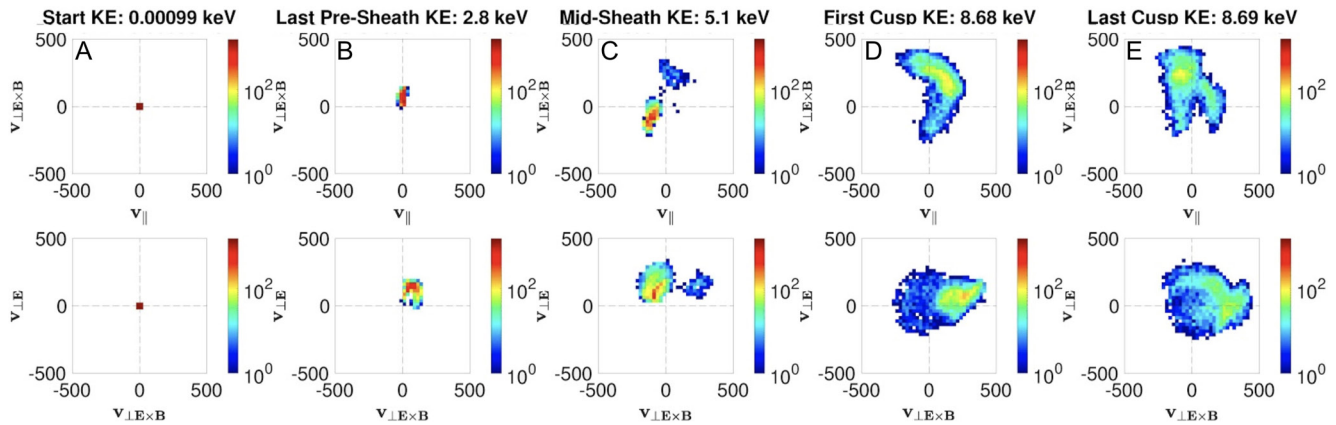


Figure 8. 3D velocity distribution function (VDF; in km/s) of Type 0 ions at key locations. The top panel of each column is the ions' VDF in the B (parallel) and $E \times B$ plane, and the bottom is the ions' VDF in the two perpendicular directions, $E \times B$ and $B \times E \times B = E$.

4. Discussion: Energy Distribution Function

As demonstrated by the significant differences in population type and frequency between the two simulations we analyzed, upstream conditions play a significant role in which dayside Na^+ energization mechanism dominates. We are therefore unfortunately limited in our ability to study the energization of sodium with FIPS alone, as its measurements cannot be placed into an upstream context due to the lack of an upstream monitor. However, given that the BepiColombo mission will permit simultaneous observations of upstream conditions and magnetospheric heavy ions like Na^+ as soon as the year 2026, it is important to ensure that our model permits effective comparison to data when simultaneous measurements of the cusp and of upstream conditions similar to our representative examples are made.

To this end, we have developed the capability to process AMPS output data into a 3D energy distribution function. In order to visualize these ions in a scientifically meaningful 3D space, we define a coordinate space with a “parallel” direction pointed along the magnetic field direction, one of two perpendicular directions pointed along $E \times B$, which is perpendicular to the parallel (B) direction by definition, and a second perpendicular direction pointed along $B \times (E \times B)$ to complete the right-handed system. Conveniently, because the electric field is defined as $E = -U \times B$ in our model and therefore definitionally perpendicular to B , the second perpendicular direction is equivalent to the E field direction. In Figure 8, we have plotted the VDF (velocity distribution function) of Type 0 ions in this coordinate system at the five key points along a Type 0 ion's trajectory identified in Figure 3.

In the leftmost (a) column of Figure 8, we have plotted the VDF at the Type 0 ions' generation, consistent with location A in Figure 3. At this point, all the ions should have exactly 1 eV of energy, which is confirmed in the average energy displayed in the column title. In the second (b) column, we have aggregated the velocity distribution of Type 0 ions as they arrive at the magnetopause. As is apparent in the top plot of column b, where v_{\parallel} on the horizontal axis in km/s is contrasted with $v_{\perp E \times B}$ on the vertical axis, these ions are preferentially accelerated in the perpendicular direction as expected due to pickup. As they move in this direction, they gain perpendicular energy which increases their gyroradius, causing them to gyrate out of the magnetosphere into the sheath, in trajectories of the variety seen in Figure 3.

Per the third (c) column, taken at the midpoint in each ion's first traversal of the magnetosheath, these ions undergo significant energization due to pickup in the magnetosheath, evident in their bulk speed approaching the speed of the local magnetosheath flow. Additionally, their location in the perpendicular plane has changed since just before they cross into the sheath. This is likely a combination of the acceleration they experience and the changing magnetic field orientation between the two spatial locations.

By the time these ions have moved into the cusp, they attain nearly 10 keV of energy on average, as can be seen in the fourth (d) column, displaying the VDF of these ions as they arrive at the cusp. The final (e) column shows the ions' VDF as they are exiting the cusp. Although there is a significant change in the

distribution in both planes relative to when the ions entered the cusp, it is notable that the average energy of this population is unchanged through the cusp, as can be seen in the titles of the final two columns. Although these ions have predominantly positive v_{\parallel} as they enter the cusp in column (d), they have predominantly negative v_{\parallel} as they exit the cusp in the (e) column. This is consistent with the expectation that these ions bounce in the cusp, moving along field lines toward the cusp on their way in, and moving along field lines away from the cusp and toward the magnetotail as they exit.

5. Conclusions

The FIPS instrument aboard MESSENGER consistently observed singly charged sodium ions at energies of between 1 and 13 keV in Mercury's northern planetary cusp (Raines et al., 2014). This was a big surprise since these ions are likely generated at or less than 1 eV. Because no known acceleration mechanism local to the cusp can account for this energy gain, we set out in search of a plausible explanation for Na^+ energization of 3–4 orders of magnitude in the short distance between generation and cusp traversal.

Through kinetic simulation of particle trajectories through the electric and magnetic fields output from a global MHD model of Mercury's magnetosphere, we build upon our understanding Na^+ energization through two crucial results. The first core result of our modeling work is the demonstration that Na^+ ions generated in the closed field region are quickly energized by the local convective electric field to the order of hundreds of eV. Some of the ions generated in the closed field region move directly from this region to the cusp (Type 1 ions). Under the external conditions imposed in our MHD modeling, these Type 1 ions are a convincing match to mission-averaged FIPS Na^+ cusp observations.

Other ions generated in the closed field region and accelerated by the local flow gain sufficient energy and are aligned appropriately to escape this region into the sheath (Type 0 ions). By examination of these Type 0 ions, we establish the second major conclusion of this work—that a two-step energization mechanism, where the second step is further and significant energization in the sheath, can account for Na^+ energized up to and beyond the limit of FIPS' upper energy threshold. Taken together, these results show that both one- and two-stage ion pickup processes can account for the energies of many of the Na^+ ions observed in Mercury's northern magnetospheric cusp by MESSENGER in previous work.

Although we do not perform any specific estimate of the cross-magnetospheric potential in either of our simulation outputs, it is notable that the average energy of the ions observed by FIPS is the same order of magnitude as the average cross-magnetospheric potential of 19 kV reported in Jasinski et al. (2017). However, our findings on the potency of the energization process inside the closed field region, causing ions to gyrate out of the dayside magnetopause, almost certainly preclude the hypothesis that FIPS observed significant densities of Na^+ ions in the cusp that were energized in the tail. The gyroradius of an ion with the mass of sodium with the necessary keV energies would be on the order of hundreds to thousands of kilometers, which would give such ions little opportunity to gain access to the cusp following any energization in the tail that was as rapid and effective as the dayside processes we analyzed.

Through an order-of-magnitude comparison and analysis to MESSENGER observations, we establish that the Dungey cycle return flow in the dayside closed field region and the magnetosheath flow provide sufficient free energy for pickup to explain FIPS observations of keV cusp ions. However, a more detailed sensitivity analysis of simulation parameters compared to realistic conditions at Mercury and a refinement of mission-averaged sodium data permitting direct comparison of similar observed and modeled conditions would both be necessary in order to conclusively predict that pickup is responsible for the energization of Na^+ into Mercury's northern cusp. Ultimately, data from the multispacecraft BepiColombo mission, taken when one spacecraft was observing upstream conditions and the other observing dayside and cusp conditions, will be necessary to confirm such a prediction.

Data Availability Statement

Both the BATSRUS and AMPS codes are publicly available for download as a component of the Space Weather Modeling Framework from the Center for Space Environment Modeling at the University of Michigan (<http://csem.engin.umich.edu/tools/swmf/>). FIPS and MAG data are publicly available

for download through the NASA Planetary Data System MESSENGER EPPS repository at <https://doi.org/10.17189/1519742>.

Acknowledgments

This work was supported by NASA First Investigators in NASA Earth and Space Science and Technology (FINESST) grant 80NSSC19K1526 and by NASA Discovery Data Analysis Program (DDAP) grants NNX15AL01G and 80NSSC20K1148. S. Aizawa acknowledges the support of CNES for the BepiColombo mission.

References

- Anderson, B. J., Acuña, M. H., Lohr, D. A., Scheifele, J., Ravall, A., Korth, H., & Slavin, J. A. (2007). The magnetometer instrument on MESSENGER. *Space Science Reviews*, 131(1), 417–450. <https://doi.org/10.1007/s11214-007-9246-7>
- Anderson, B. J., Johnson, C. L., Korth, H., Purucker, M. E., Winslow, R. M., Slavin, J. A., et al. (2011). The global magnetic field of Mercury from MESSENGER orbital observations. *Science*, 333(6051), 1859–1862. <https://doi.org/10.1126/science.1211001>
- Andrews, G. B., Zurbuchen, T. H., Mauk, B. H., Malcom, H., Fisk, L. A., Gloeckler, G., et al. (2007). The energetic particle and plasma spectrometer instrument on the MESSENGER spacecraft. *Space Science Reviews*, 131(1), 523–556. <https://doi.org/10.1007/s11214-007-9272-5>
- Cassidy, T. A., & Johnson, R. E. (2005). Monte Carlo model of sputtering and other ejection processes within a regolith. *Icarus*, 176(2), 499–507. <https://doi.org/10.1016/j.icarus.2005.02.013>
- Cowley, S. W. H., & Owen, C. J. (1989). A simple illustrative model of open flux tube motion over the dayside magnetopause. *Planetary and Space Science*, 37(11), 1461–1475. [https://doi.org/10.1016/0032-0633\(89\)90116-5](https://doi.org/10.1016/0032-0633(89)90116-5)
- Delcourt, D. C., Grimald, S., Leblanc, F., Berthelier, J.-J., Millilo, A., Mura, A., et al. (2003). A quantitative model of the planetary Na⁺ contribution to Mercury's magnetosphere. *Annales Geophysicae*, 21(8), 1723–1736. <https://doi.org/10.5194/angeo-21-1723-2003>
- Delcourt, D. C., Moore, T. E., Orsini, S., Millilo, A., & Sauvaud, J.-A. (2002). Centrifugal acceleration of ions near Mercury. *Geophysical Research Letters*, 29(12), 1591. <https://doi.org/10.1029/2001GL013829>
- Delcourt, D. C., Seki, K., Terada, N., & Miyoshi, Y. (2005). Electron dynamics during substorm dipolarization in Mercury's magnetosphere. *Annales Geophysicae*, 23(10), 3389–3398. <https://doi.org/10.5194/angeo-23-3389-2005>
- Delcourt, D. C., Seki, K., Terada, N., & Moore, T. E. (2012). Centrifugally stimulated exospheric ion escape at Mercury. *Geophysical Research Letters*, 39, L22105. <https://doi.org/10.1029/2012GL054085>
- DiBraccio, G. A., Slavin, J. A., Boardson, S. A., Anderson, B. J., Korth, H., Zurbuchen, T. H., et al. (2013). MESSENGER observations of magnetopause structure and dynamics at Mercury. *Journal of Geophysical Research: Space Physics*, 118, 997–1008. <https://doi.org/10.1002/jgra.50123>
- Dungey, J. W. (1961). Interplanetary magnetic field and the auroral zones. *Physical Review Letters*, 6(2), 47–48. <https://doi.org/10.1103/PhysRevLett.6.47>
- Fougere, N., Altwegg, K., Berthelier, J.-J., Bieler, A., Bockelée-Morvan, D., Calmonte, U., et al. (2016). Three-dimensional direct simulation Monte-Carlo modeling of the coma of comet 67P/Churyumov-Gerasimenko observed by the VIRTIS and ROSINA instruments on board Rosetta. *Astronomy & Astrophysics*, 588, A134. <https://doi.org/10.1051/0004-6361/201527889>
- Gombosi, T. I., Tóth, G., De Zeeuw, D. L., Hansen, K. C., Kabin, K., & Powell, K. G. (2002). Semirelativistic magnetohydrodynamics and physics-based convergence acceleration. *Journal of Computational Physics*, 177(1), 176–205. <https://doi.org/10.1006/jcph.2002.7009>
- Jasinski, J. M., Slavin, J. A., Raines, J. M., & DiBraccio, G. A. (2017). Mercury's solar wind interaction as characterized by magnetospheric plasma mantle observations with MESSENGER. *Journal of Geophysical Research: Space Physics*, 122, 12153–12169. <https://doi.org/10.1002/2017JA024594>
- Jia, X., Hansen, K. C., Gombosi, T. I., Kivelson, M. G., Tóth, G., DeZeeuw, D. L., & Ridley, A. J. (2012). Magnetospheric configuration and dynamics of Saturn's magnetosphere: A global MHD simulation. *Journal of Geophysical Research*, 117, A05225. <https://doi.org/10.1029/2012JA017575>
- Jia, X., Kivelson, M. G., & Gombosi, T. I. (2012). Driving Saturn's magnetospheric periodicities from the upper atmosphere/ionosphere. *Journal of Geophysical Research*, 117, A04215. <https://doi.org/10.1029/2011JA017367>
- Jia, X., Slavin, J. A., Gombosi, T. I., Daldorff, L. K. S., Toth, G., & van der Holst, B. (2015). Global MHD simulations of Mercury's magnetosphere with coupled planetary interior: Induction effect of the planetary conducting core on the global interaction. *Journal of Geophysical Research: Space Physics*, 120, 4763–4775. <https://doi.org/10.1002/2015JA021143>
- Jia, X., Slavin, J. A., Poh, G., DiBraccio, G. A., Toth, G., Chen, Y., et al. (2019). MESSENGER observations and global simulations of highly compressed magnetosphere events at Mercury. *Journal of Geophysical Research: Space Physics*, 124, 229–247. <https://doi.org/10.1029/2018JA026166>
- Kallio, E., & Janhunen, P. (2003). Solar wind and magnetospheric ion impact on Mercury's surface. *Geophysical Research Letters*, 30(17), 1877. <https://doi.org/10.1029/2003GL017842>
- Leblanc, F., & Johnson, R. E. (2003). Mercury's sodium exosphere. *Icarus*, 164(2), 261–281. [https://doi.org/10.1016/S0019-1035\(03\)00147-7](https://doi.org/10.1016/S0019-1035(03)00147-7)
- Ma, Y., Nagy, A. F., Hansen, K. C., DeZeeuw, D. L., Gombosi, T. I., & Powell, K. G. (2002). Three-dimensional multispecies MHD studies of the solar wind interaction with Mars in the presence of crustal fields. *Journal of Geophysical Research*, 107(A10), 1282. <https://doi.org/10.1029/2002JA009293>
- Möbius, E., Hovestadt, D., Klecker, B., Scholer, M., Gloeckler, G., & Ipavich, F. M. (1985). Direct observation of He⁺ pick-up ions of interstellar origin in the solar wind. *Nature*, 318(6045), 426–429. <https://doi.org/10.1038/318426a0>
- Najib, D., Nagy, A. F., Tóth, G., & Ma, Y. (2011). Three-dimensional, multifluid, high spatial resolution MHD model studies of the solar wind interaction with Mars. *Journal of Geophysical Research*, 116, A05204. <https://doi.org/10.1029/2010JA016272>
- Newell, P. T., & Meng, C.-I. (1988). Hemispherical asymmetry in cusp precipitation near solstices. *Journal of Geophysical Research*, 93(A4), 2643–2648. <https://doi.org/10.1029/JA093iA04p02643>
- Paschalidis, N. P., Sarris, E. T., Krimigis, S. M., McEntire, R. W., Levine, M. D., Daglis, I. A., & Anagnostopoulos, G. C. (1994). Energetic ion distributions on both sides of the Earth's magnetopause. *Journal of Geophysical Research*, 99(A5), 8687–8703. <https://doi.org/10.1029/93JA03563>
- Powell, K. G., Roe, P. L., Linde, T. J., Gombosi, T. I., & De Zeeuw, D. L. (1999). A solution-adaptive upwind scheme for ideal magnetohydrodynamics. *Journal of Computational Physics*, 154(2), 284–309. <https://doi.org/10.1006/jcph.1999.6299>
- Raines, J. M., Gershman, D. J., Slavin, J. A., Zurbuchen, T. H., Korth, H., Anderson, B. J., & Solomon, S. C. (2014). Structure and dynamics of Mercury's magnetospheric cusp: MESSENGER measurements of protons and planetary ions. *Journal of Geophysical Research: Space Physics*, 119, 6587–6602. <https://doi.org/10.1002/2014JA020120>
- Sarkango, Y., Jia, X., & Toth, G. (2019). Global MHD simulations of the response of Jupiter's magnetosphere and ionosphere to changes in the solar wind and IMF. *Journal of Geophysical Research: Space Physics*, 124, 5317–5341. <https://doi.org/10.1029/2019JA026787>

- Shue, J.-H., Chao, J. K., Fu, H. C., Russell, C. T., Song, P., Khurana, K. K., & Singer, H. J. (1997). A new functional form to study the solar wind control of the magnetopause size and shape. *Journal of Geophysical Research*, 102(A5), 9497–9511. <https://doi.org/10.1029/97JA00196>
- Siscoe, G. L., Ness, N. F., & Yeates, C. M. (1975). Substorms on Mercury? *Journal of Geophysical Research*, 80(31), 4359–4363. <https://doi.org/10.1029/JA080i031p04359>
- Slavin, J. A., Acuña, M. H., Anderson, B. J., Baker, D. N., Benna, M., Boardsen, S. A., et al. (2009). MESSENGER observations of magnetic reconnection in Mercury's magnetosphere. *Science*, 324(5927), 606–610. <https://doi.org/10.1126/science.1172011>
- Slavin, J. A., Anderson, B. J., Baker, D. N., Benna, M., Boardsen, S. A., Gloeckler, G., et al. (2010). MESSENGER observations of extreme loading and unloading of Mercury's magnetic tail. *Science*, 329(5992), 665–668. <https://doi.org/10.1126/science.1188067>
- Slavin, J. A., DiBraccio, G. A., Gershman, D. J., Imber, S. M., Poh, G. K., Raines, J. M., et al. (2014). MESSENGER observations of Mercury's dayside magnetosphere under extreme solar wind conditions. *Journal of Geophysical Research: Space Physics*, 119, 8087–8116. <https://doi.org/10.1002/2014JA020319>
- Slavin, J. A., & Holzer, R. E. (1981). Solar wind flow about the terrestrial planets 1. Modeling bow shock position and shape. *Journal of Geophysical Research*, 86(A13), 11401–11418. <https://doi.org/10.1029/JA086iA13p11401>
- Smith, M. F., & Lockwood, M. (1996). Earth's magnetospheric cusps. *Reviews of Geophysics*, 34(2), 233–260. <https://doi.org/10.1029/96RG00893>
- Solomon, S. C., McNutt, R. L., Gold, R. E., & Domingue, D. L. (2007). MESSENGER mission overview. *Space Science Reviews*, 131(1), 3–39. <https://doi.org/10.1007/s11214-007-9247-6>
- Tenishev, V., Combi, M., & Davidsson, B. (2008). A global kinetic model for cometary comae: The evolution of the coma of the Rosetta target comet Churyumov-Gerasimenko throughout the mission. *The Astrophysical Journal*, 685(1), 659–677. <https://doi.org/10.1086/590376>
- Tenishev, V., Combi, M.-R., Jia, X., Rubin, M., & Raines, J. (2013). Kinetic modeling of the sodium distribution in the Hermean surface-bound exosphere. In *AAS/Division for Planetary Sciences Meeting Abstracts* (Vol. 45, p. 114.02).
- Tenishev, V., Shou, Y., Borovikov, D., Lee, Y., Fougere, N., Michael, A., & Combi, M. R. (2021). Application of the Monte Carlo method in modeling dusty gas, dust in plasma, and energetic ions in planetary, magnetospheric, and heliospheric environments. *Journal of Geophysical Research: Space Physics*, 126, e2020JA028242. <https://doi.org/10.1029/2020JA028242>
- Tóth, G., van der Holst, B., Sokolov, I. V., De Zeeuw, D. L., Gombosi, T. I., Fang, F., et al. (2012). Adaptive numerical algorithms in space weather modeling. *Journal of Computational Physics*, 231(3), 870–903. <https://doi.org/10.1016/j.jcp.2011.02.006>
- Winslow, R. M., Anderson, B. J., Johnson, C. L., Slavin, J. A., Korth, H., Purucker, M. E., et al. (2013). Mercury's magnetopause and bow shock from MESSENGER magnetometer observations. *Journal of Geophysical Research: Space Physics*, 118, 2213–2227. <https://doi.org/10.1002/jgra.50237>
- Yagi, M., Seki, K., Matsumoto, Y., Delcourt, D. C., & Leblanc, F. (2017). Global structure and sodium ion dynamics in Mercury's magnetosphere with the offset dipole. *Journal of Geophysical Research: Space Physics*, 122, 10990–11002. <https://doi.org/10.1002/2017JA024082>
- Zurbuchen, T. H., Gloeckler, G., Cain, J. C., Lasley, S. E., & Shanks, W. (1998). Low-weight plasma instrument to be used in the inner heliosphere. In *Proceedings of SPIE* (Vol. 3442). <https://doi.org/10.1117/12.330260>
- Zurbuchen, T. H., Raines, J. M., Slavin, J. A., Gershman, D. J., Gilbert, J. A., Gloeckler, G., et al. (2011). MESSENGER observations of the spatial distribution of planetary ions near Mercury. *Science*, 333(6051), 1862–1865. <https://doi.org/10.1126/science.1211302>